GeoScienceWorld
Lithosphere
Volume 2022, Article ID 5922501, 14 pages
https://doi.org/10.2113/2022/5922501

Lithosphere

Research Article

Experimental Study on Failure Model of Tailing Dam Overtopping under Heavy Rainfall

Guangjin Wang,[1,2,3,4] **Bing Zhao**,[1,2] **Rong Lan**,[5] **Dianwen Liu**,[1,3] **Bisheng Wu**,[4] **Yaoji Li**,[6] **Quanming Li**,[7] **Hanmin Zhou**,[8] **Mingsheng Liu**,[5] **Wenlian Liu**,[9] **and Xinjie Liu**[1,2]

[1]*Faculty of Land Resources Engineering, Kunming University of Science and Technology, Kunming 650093, China*
[2]*Yunnan International Technology Transfer Center for Mineral Resources Development and Solid Waste Resource Utilization, Kunming 650093, China*
[3]*Yunnan Key Laboratory of Green Separation and Enrichment of Strategic Mineral Resources, Kunming 650051, China*
[4]*State Key Laboratory of Hydroscience and Engineering, Department of Hydraulic Engineering, Tsinghua University, Beijing 100084, China*
[5]*Kunming Engineering & Research Institute of Nonferrous Metallurgy Co., Ltd., Kunming 650051, China*
[6]*Yunnan Phosphate Chemical Group Co., Ltd., Kunming 650600, China*
[7]*School of Civil Engineering, North China University of Technology, Beijing 100144, China*
[8]*General Research Institute of Mining & Metallurgy Technology Group, Beijing 100160, China*
[9]*China Nonferrous Metals Industry Kunming Survey and Design Research Institute Co., Ltd., Kunming 650051, China*

Correspondence should be addressed to Bing Zhao; b912681848z@163.com

Received 31 March 2022; Revised 23 September 2022; Accepted 1 October 2022; Published 14 November 2022

Academic Editor: Manchao He

Unusual rainfall is the primary cause of the failure of the tailing dams, and overtopping is the most representative model of the tailing dam failure. The upstream tailing dam was selected as the research object to study the whole process of breach extension and the overtopping dam-failure mechanism under the full-scale rainfall condition. The results showed that the significant size grading phenomenon in the front, middle, and end of the tailing pond was obvious due to the flow separation effect, and its average particle diameter was D50. At different moments of rainfall, the height of the infiltration line at different positions of the dam body was different; at the rainfall of 3600 s, the height of the infiltration line lagged behind the height of the tailing pond, and this phenomenon from the tail of pond to the outside of the dam slope became more obvious. After the rainfall of 3600 s, the height of the infiltration line lagging behind the water level in the pond basically disappeared, and the rate of infiltration line rise kept pace with the rate of water level. The process of overtopping dam-failure experienced dam overtopping (gully erosion), formation of a multistepped small "scarp," breach rapid expansion, formation of large "scarp," and burst (fan-shaped formation). The width and depth of the breach showed a positive correlation, and the widening rate of the breach was 3 to 8 times of the deepening rate, especially in the middle of the dam break, widening behavior occupied the dominant factor. The shape of the dam body after failure was parabolic, and the dam body had obvious elevation changes. These results provide the theoretical guidance and engineering application value for improving the theory and early warning model of the upstream tailing dam.

1. Introduction

The tailing dam is a major source of danger with high potential energy. Once the dam breaks, it will seriously endanger the life and property safety of the residents in the downstream areas and cause serious environmental and ecological damage at the same time [1–3]. The stability of the tailing pond is closely related to the seepage law [4], damage characteristics [5–7], and failure characteristics [8–10] of the surrounding rock.

At present, more than 90% of tailing dams in China are built by using the upstream construction method, and

upstream tailing dams have the characteristics of complex dam body structure, high infiltration line, and complex dam failure mechanism [11–17]. Therefore, it is necessary to investigate the failure mechanism of the tailing dam and provide technology support supporting for safety monitoring and controlling.

Rico et al. [18] counted 218 tailing dam failure accidents in the world from 1910 to 2009. The analysis showed that the primary cause of tailing dam failures was unusual rainfall, and about 76% of tailing dam failures were selected for the upstream construction method. Aiming at the problem of tailing dam failure under rainfall conditions, Zandarín et al. [19] carried out research on the infiltration mechanism of tailing dam slopes under rainfall conditions, established a corresponding calculation model under rainfall, and analyzed its infiltration line and its influence on the stability of the dam body. Lade and Yamamuro and Anderson [20, 21] studied the static liquefaction characteristics of granular materials and pointed out that tailing material belongs to noncohesive or less cohesive bulk soil, which makes it easy to liquefy. Rico et al. [18] established the relationship between the geometric parameters of tailing dam (dam height, storage capacity, etc.) and tailing fluid characteristics. The relationships between soil erosion degree and flow rate, steep sill height, and soil parameters were proposed. Hanson et al. [22] analyzed the formation and development process of the dam body rupture through field and laboratory simulating experiments. Debarghya and Deepamkar et al. [23] carried out the experiment on tailing dam failure under earthquake and pointed out that tailing liquefaction during the earthquake was the main reason for the instability of tailing pond.

In terms of tailing dam stability and dam failure prediction model, Zandarín et al. and Gens and Alonso [19, 24] studied the variation law of tailing pond slope stability under different rainfall conditions and proposed a progressive failure model for the tailing dam. Salgueiro et al. [25] used the observation data before the disaster accident and the accident consequences to assess the risk of dam failure of the tailing pond. Wang et al. [26] adopted the satellite remote sensing digital surface model data and advanced meshless smoothed particle hydrodynamics method to study the run-out tailing slurry routing across real downstream terrains affected by dam failures. Zhuang et al. [27] studied the rheological properties and mechanism of the tailing slurry from initiation to run-out through a dynamic model and rheology tests.

Although the stability monitoring technology is relatively mature, the prediction of tailing dam instability exists because of the complex and changeable factors and interaction effect [28–32]. There is still a lack of relevant theoretical foundations in the safety diagnosis system of tailing dams, especially in terms of the dam collapse mechanism under unusual rainfall conditions. More relevant dam failure experimental data are needed to supplement and improve its prediction and early warning model. There are three main reasons for the flooding of tailing ponds [33–35]. First, the flood control capacity of tailing ponds is insufficient, including insufficient flood regulation storage capacity [36–38], and the cross-section of flood discharge facilities is too small or damaged or blocked. The second is excessive floods (experiences above the fortification standard), causing floods to overflow the top of the dam [39]. The third is improper management or emergency measures.

Table 1: Similar scale of the model.

Similar parameters	Length	Gravitational acceleration	Flow	Velocity
Similarity ratio	1 : 150	1 : 1	$1:150^{5/2}$	$1:150^{1/2}$

Therefore, this research took the upstream tailing dam as the research object, adopted a self-designed tailing dam failure test device, and used indoor model experiments and theoretical analysis methods to study the indoor tailing dam pile under unusual rainfall conditions. Systematic observation and research were made on the tailing deposition law under the condition of scattered ore drawing in front of the dam, the change of saturation line of tailing dam under rainfall, the mechanism of tailing dam overtopping, and the whole process of its breach expansion under rainfall, which overcame the influence of the traditional small-scale model test on the scale of the model, improved the spatiotemporal dynamic evolution mechanism of tailing dam overtopping and breach under rainfall and flood conditions, and laid a solid theoretical foundation for further establishing the relationship between the dynamic development process of the breach and the change of sand flow. It will have strong engineering guiding significance in the future.

2. Similar Simulation Test Scheme

2.1. Determination of Similar Condition. The collapse process of tailing pond is extremely complex, which involves many factors such as hydraulics, soil mechanics, and sediment transport mechanics characteristics. Similarity relationships derived from various factors are often incompatible, and experimental models cannot satisfy all similarity conditions. Therefore, following the similarity principle [40], the main force is selected for analysis. The prototype tailing pond of the model is located in Huili County, Sichuan Province, China. The designed total dam height of the tailing pond is 92 m, including the initial dam height of 32 m and the accumulation dam of 60 m. The pool water area of the tailing pond is 7.65 km^2, the total storage capacity of the tailing pond is 10,918,100 m^3, the effective storage capacity is 9,826,200 m^3, and the tailing pond is classified as grade III. The similarity conditions are determined as shown in Table 1.

To ensure the similarity of main mechanical properties between the material used in the experiment and prototype material, as well as the reliability of experimental results, the viscosity of the model sand and the prototype sand must be similar. According to the selection principle of model sand, the physical and mechanical characteristics of the model sand and the prototype sand are far from each other. Therefore, the model materials are all prototype tailing sand, and the particle size distribution curve of prototype tailing sand is shown in Figure 1.

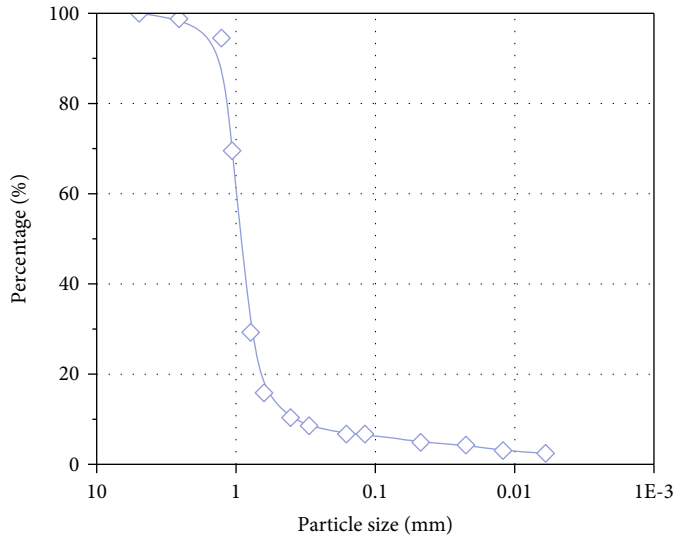

Figure 1: Particle size distribution curve of prototype tailing sand.

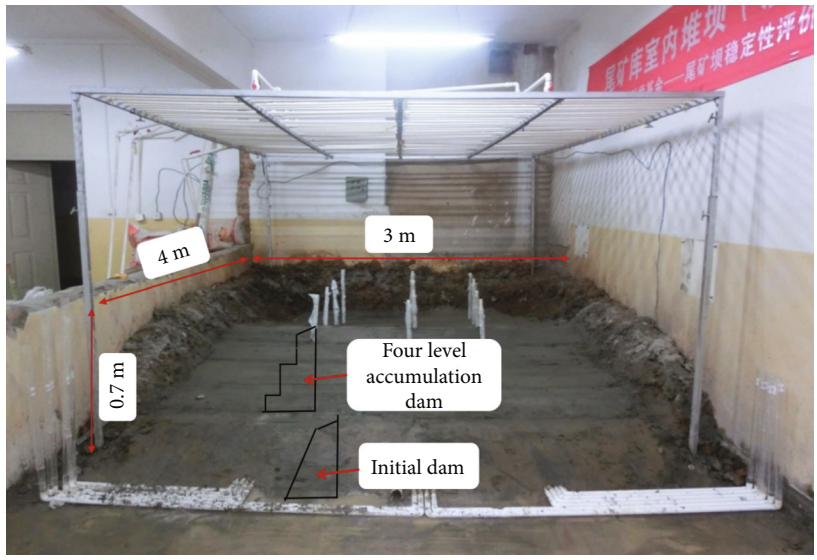

Figure 2: Indoor accumulation model of tailing dam.

2.2. Indoor Dam Model. The valley-type upstream tailing pond was selected as the research model for the indoor model test. The three sides of the model were poured into a clay wall. The size of the model is 4 m in length and 3 m in width, and the height of the clay wall is 0.7 m. The indoor dam model is shown in Figure 2.

2.3. Experiment System. The indoor model experimental system of the tailing dam is shown in Figure 3. The system device mainly includes the following: (1) rainfall system: the rainfall system adopts a spray (pipe network) rainfall device to simulate rainfall, and it can record the variation law of rainfall with time (as shown in Figure 3(a)); (2) monitoring system: the system includes dam displacement monitoring, infiltration line monitoring, reservoir water level monitoring, and an automatic camera system. The monitoring equipment can record the development of the dam body over time during the experiment, and the camera can record the entire instability and disaster process of the tailing dam (as shown in Figures 3(a) and 3(b)); and (3) transport system: tailing manufacture and mixing equipment (as shown in Figure 3(a)).

2.3.1. Rainfall System. For this experiment, the tailing dam model is rectangular in size and large in area. If the circular sprinkler covers the whole area, it will inevitably cause rainfall overlap, which will lead to a big difference in rainfall intensity and affect rainfall uniformity. Therefore, in this experiment, the rainfall device adopts spray (pipe network) rainfall mode, as shown in Figure 4, and the rainfall uniformity test is carried out. Eight measuring points were arranged in the rainfall area, and the measuring time of each measuring point was 2 minutes. The received rainwater was poured into a measuring cylinder to measure its volume and

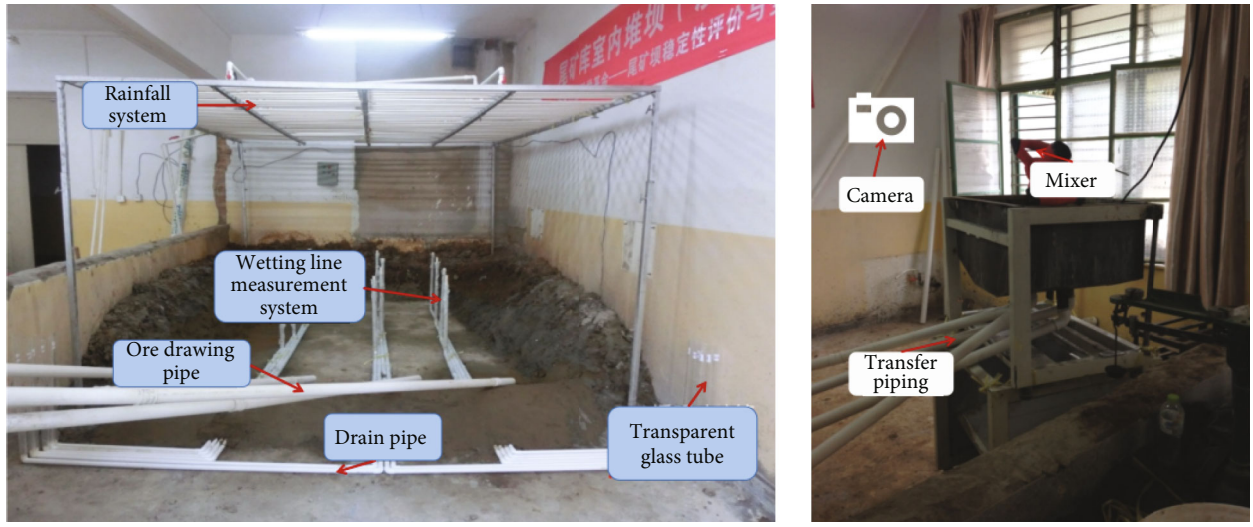

Figure 3: Experiment system: (a) rainfall and monitor device and (b) tailing transport and blender device.

Figure 4: Rainfall system.

then converted into rainfall. Secondly, the data were measured in turn, and according to the rainfall of each measuring point, the uniformity Equation (1) was used to calculate.

$$k = 1 - \sum_{i=1}^{n} \frac{|x_i - \bar{x}|}{n\bar{x}}. \quad (1)$$

In the above equation, k is the uniformity coefficient, x_i is the rainfall intensity of the measuring point, x is the average rainfall intensity of each measuring point, and n is the number of measuring points.

At present, the uniformity index of rainfall simulation devices in China is generally greater than 0.8. The uniformity is calculated to be 0.82, which is larger than the required value of 0.80 and meets the requirements.

2.3.2. Measuring Device for Infiltration Line. Three rows of PVC vertical water filter pipes with a diameter of 25 mm were arranged along the ditch in the dam model. The bottom of the water filter pipes was connected with the PVC pipe, and the PVC pipe is connected with the transparent glass tube outside the model dam, as shown in Figure 3(a). Through the water level scale of the glass tube outside the model dam, the height of the infiltration line in the tailing pond model can be determined. The height of the infiltration line at four points is measured in each section, and the four vertical water filter pipes of three rows pipes are marked 1-1, 1-2, 1-3, 1-4, 2-1, 2-2, 2-3, 2-4, 3-1, 3-2, 3-3, and 3-4, respectively. The X, Y, Z coordinate system was marked as shown in Figure 5.

2.3.3. Displacement Monitoring System of Tailing Dam Body. Combined with the actual situation of the dam body, 4 transverse profile monitoring lines on the dam body were installed for the displacement monitoring of the dam body in this model (that is, a profile was set at the dam bottom of each subdam). The displacement monitoring system

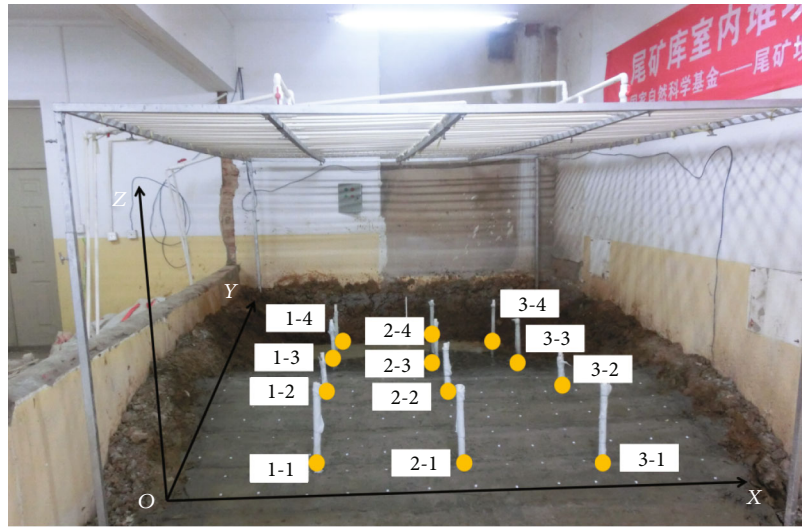

Figure 5: Arrangement of infiltration line piping.

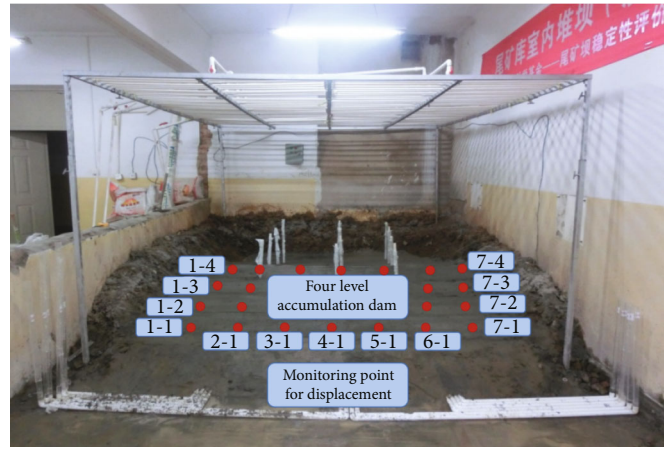

Figure 6: Distribution of the displacement monitoring points.

included 4 monitoring sections, and each profile included 7 monitoring points, with a total of 28 monitoring points, namely, 1-1~7-1 transverse section, 1-2~7-2 transverse section, 1-3~7-3 transverse section, and 1-4 ~ 7-4 transverse section (as shown in Figure 6). At the same time, a fixed displacement reference line corresponding to the dam body was set on the wall surface, and the distance between the fixed reference line and measurement point on the dam body slope was measured by a laser range finder. Therefore, the displacement variation before and after the dam body collapses can be obtained.

3. Results and Discussion

3.1. Particle Deposition Law of Tailings in the Front Dam. The engineering properties of tailings are closely related to the deposition characteristics. The deposition of tailings is mainly determined by factors such as the particle size distribution, discharge method, and the concentration of tailing slurry and topography. To obtain the particle size deposition law of the scattered discharge tailings in the front dam, the method of discharge tailings was shown in Figure 7(a). It could be seen from Figure 7(b) that the tailings had no obvious sedimentary tailing sand when the tailing slurry flowed into the tailing pond. It was worth noting that the tailing slurry flowed into the tailing pond in the state of "thin flow" and "laminar flow," forming a clear fan-shaped alluvial beach in the front dam.

To reflect the deposition law of tailing particle on the dry beach, the front (0.2 m away from the subdam), middle (middle of the dry beach), and tail (0.2 m from the water level) of the tailings of tailing pond were taken along the middle line of the fourth-level subdam after the dam was built. Three groups of tailings were taken for particle size analysis, and the comparison curves of particle size distribution are shown in Figure 8.

It can be clearly drawn that the particle size of the tailings in front of, in, and at the end of the tailing pond is quite different from the experimental analysis. Where the particle size of tailings in front of the tailing pond was D50 = 0.11 mm, the particle size of tailings in the tailing pond was D50 = 0.051 mm, and the particle size behind

Figure 7: Particle size distribution of tailings: (a) tailing discharge and (b) particle deposition distribution.

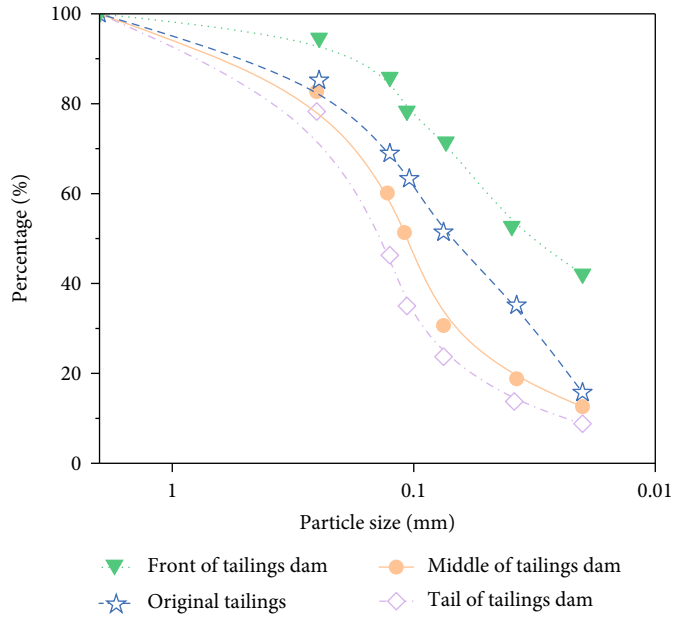

Figure 8: Tailing particle size distribution contrast curve.

the tailing pond was D50 = 0.035 mm. The tailings with a particle size of less than 0.075 mm accounted for more than 50%, which basically appeared as tailing silt and tailing mud. This deposition law of tailings is mainly related to the selecting effect of water flow. During the flow of tailing slurry on the dry beach, the coarse particles of large size settled down first, and the carrying distance affected by water flow was short. However, the fine particles of small size were carried a long distance by the water flow. Only partial particles were slowly deposited with the water flow, forming tailing silt or tailing mud to accumulate at the tail of the tailing pond. This phenomenon is also consistent with the deposition law of tailings on the dry beach in the actual engineering.

3.2. Variation Law of Infiltration Line of Dam Body. There are three main reasons for the flooding of the tailing pond: (1) the flood control capacity of the tailings pond is insufficient, including insufficient storage capacity, and the section of the flood discharge facilities is too small or damaged or blocked; (2) the overlevel flood causes floods to overflow the dam top; and (3) the improper management or emergency measures. This paper carried out a study on the dam failure process of the upstream tailing dam under rainfall conditions. During the rainfall experiment, the change of the water level with the rainfall duration in the tailing pond is shown in Figure 9.

From Figure 9, the water level continued to rise with the increase of rainfall time before the water flow in the tailing pond overflowed the top. It is because the flood discharge facilities of the tailing pond could not discharge the flood normally. The various values of the tailing pond infiltration line during different rainfall periods are shown in Figure 10.

It could be seen from Figure 10 that the height of the infiltration line of the dam body was rising as the rainfall continues, but the height variation of the infiltration line at different positions varies at different moments of the rainfall. At 0 s of rainfall, the height of the water level in the tailing pond was 10 cm, while the height of the infiltration line at the tail of the tailing pond was 5 cm, and the infiltration line at the outer slope of the dam body was 3 cm. The seepage velocity has lagged due to the pore pressure between the

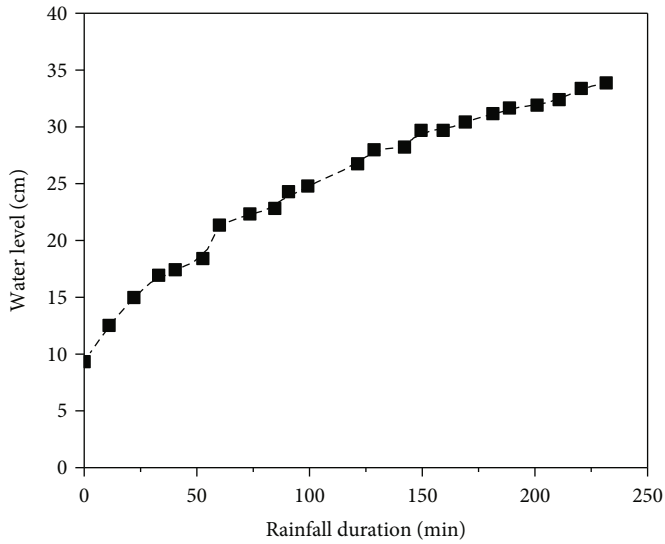

Figure 9: Water level changes with rainfall duration.

tailings particles, causing the height of the infiltration line significantly lagged behind the water level height. The phenomenon was more obvious on the outer slope of the dam body. At 3600 s of rainfall, the height of the infiltration line in front of the tailing pond and the outer slope of the dam body rose significantly, indicating that these positions were beginning to seep saturation. The phenomenon that the overall infiltration line of the dam body lagged behind the water level disappeared gradually, and the overall infiltration line of the dam body is about 19 cm. After 3600 s, the response of the infiltration line-height to the water level variation was obvious, and the rising rate of the infiltration line-height basically kept consistent with the water level height. The phenomenon that the infiltration line-height lagged behind the water level height basically disappeared. It is indicated that the water level variation in the tailing pond has a significant impact on the infiltration line height. Therefore, the water level and infiltration line should be strictly monitored when encountering heavy rainfall and floods, and the drainage and seepage measures should be adopted timely. The height of the infiltration line is controlled within the safe range to ensure the safety of the dam body.

3.3. Dam Overtopping Failure Development Process

3.3.1. Development Process of Dam Overtopping Failure. The dam-breaking mechanism of tailing ponds is very complex, involving many physical factors such as the mechanical properties of tailing materials, flooding of the dam body, and stability analysis of tailing dam. It is a problem of mutual penetration and coupling of geotechnical mechanics, hydraulics, sediment transport mechanics, and other disciplines. This experiment mainly considered the accumulation effect of particle movement in the process of tailing dam deformation. The macroscopic physical quantities were applied to illustrate the development process of dam failure and erosion. Figure 11 shows the dam collapse failure process.

From the experimental process in Figure 11, the development process of the dam body failure can be divided into the five stages:

(1) Dam Body Gully Erosion and Rupture. As shown in Figure 11(a), the overflow occurs at the top of the dam body with the increase of water level in the tailing pond. In the initial stage of overflow, the concentration of tailing sand formed by overflow is very low and close to water. With the increase of the overflow time, the small gullies initiated on the sloping surface downstream of the dam body, which merged and continuously eroded the bottom of the gully. With the continuous development of the overflow, a breach was formed in the middle of the dam.

(2) Formation of the Gully with Multistepped Small "Steep Ridges". As shown in Figure 11(b), the erosion mechanism also varied with the location. The water flow erosion occurred near the overflow of the dam crest, and the erosion caused by the accumulation of bed load appeared from downstream to the middle of the dam slope. The tailing sand erosion occurred on the bottom of the dam slope. Since the erosion rate of the bottom of the dam slope is greater than that of the top of the dam slope, the "tiny steps" were most likely to initiate form near the dam site fissure zone and eventually developed into a larger gully, which initially consists of multiple stepped small "slopes."

(3) Formation of Large "Steep Ridges" and the Development of Breach. A number of step-shaped small "steep ridges" continued to widen and develop upstream over time, and the gully finally developed into a large "steep ridge." As shown in Figure 11(c), the "slope" gradually developed upward until the upstream edge of the dam crest under the action of water flow. Afterward, the "steep ridge" continued to develop upstream, and the dam crest at the breach became lowered. The water and sand flow at the breach

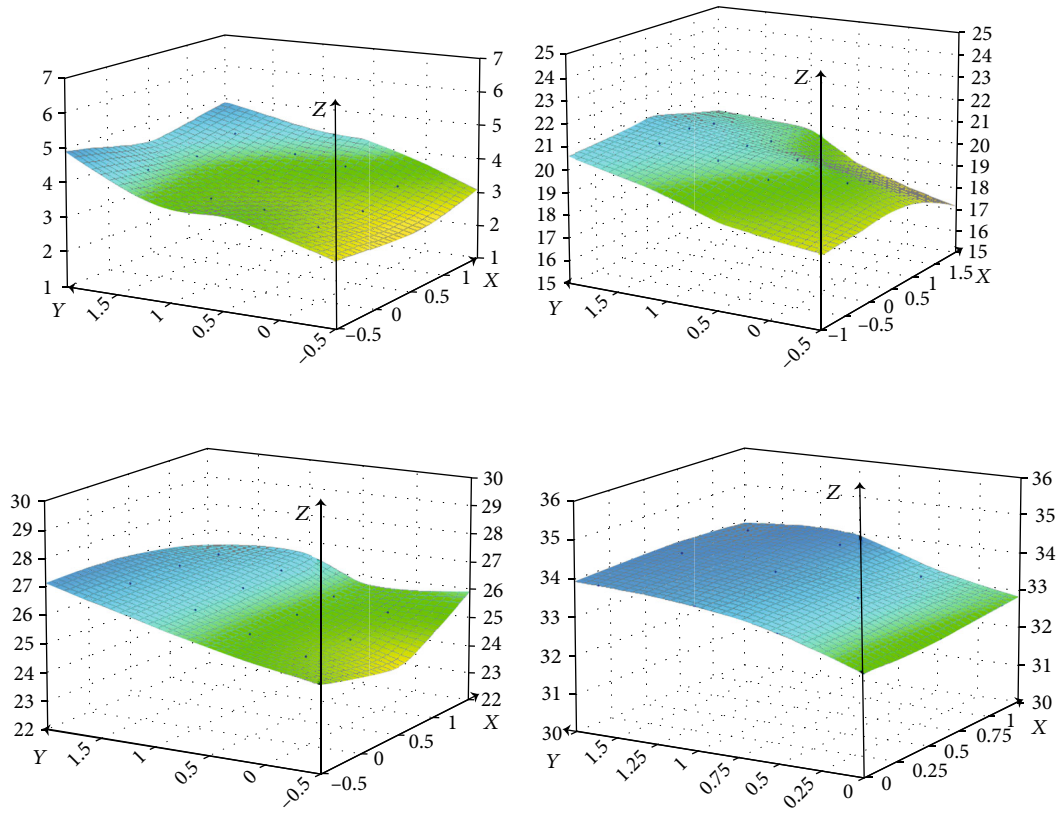

Figure 10: Three-dimensional view of rainfall infiltration surface during different periods.

increased rapidly, and the dam body was eroded by a "steep ridge," forming a "waterfall" scouring effect.

(4) Quick Development of Breach. With the increase of water and sand flow at the breach, the breach erosion became violent. The sidewall of the breach collapsed and widened, and the sediment flow reached its maximum. A large amount of sediment flow was transported downstream and accumulates in the downstream riverbed in the form of bedding, as shown in Figure 11(d).

(5) Complete Collapse of Breach. When the breach depth developed to the minimum, the development of the breach was mainly lateral expansion until the dam body completely collapsed. The sediment flows accumulated downstream after the collapse showed a fan-shaped distribution, similar to the debris flow, as shown in Figure 10(e).

3.3.2. Analysis of the Development of Ulceration Morphology. As for the breach shape, the results showed that the water first flowed over the dam crest and formed a gully on the downstream surface of the dam body and gradually develops upstream. Afterward, the initial breach formed on the dam body and body crest. For the morphological development of the breach, this research mainly focused on the development and variation of the width and depth of the breach. During the dam failure process, the depth and width of the breach (mainly refers to the breach at the dam crest) changed as shown in Table 2.

It can be seen from Table 2 that the width and depth of the breach were continuously widened laterally and deepened with the increase of the dam breach time in the process of dam failure, and the width variation was much larger than the depth variation of the breach. After dam failure, the breach was 340.58 mm in width and 63.1 mm in depth, and the width was about 5 times the depth. However, the width and deepen variation of the breach was different in different time periods. The depth and width of the breach during the dam failure process were sorted and calculated, respectively, and the variation of widening rate and deepening rate of the breach could be obtained are shown in Figure 12.

According to the development of the dam failure, the dam failure can be divided into three periods: the early period of dam failure (1~4 min of dam failure), the middle stage of dam failure (4 ~ 8 min of dam failure), and the later stage of dam failure (8~11 min of dam failure). It could be seen from Figure 12 that the widening and deepening rates of the breach were different in different periods of dam failure. In the early period, the widening and deepening rates were slow, which were corresponding to Figure 11(b). The overflow erosion was mainly at the breach, and the tailing sand was slightly scoured by the water flow because the water flow velocity was slow. A small quantity of tailing sand was transported downstream of the dam body. With the increase of the width and depth of the breach, the flow rate at the breach constantly increased, and more tailing sand was flushed to the downstream of the dam body. In the

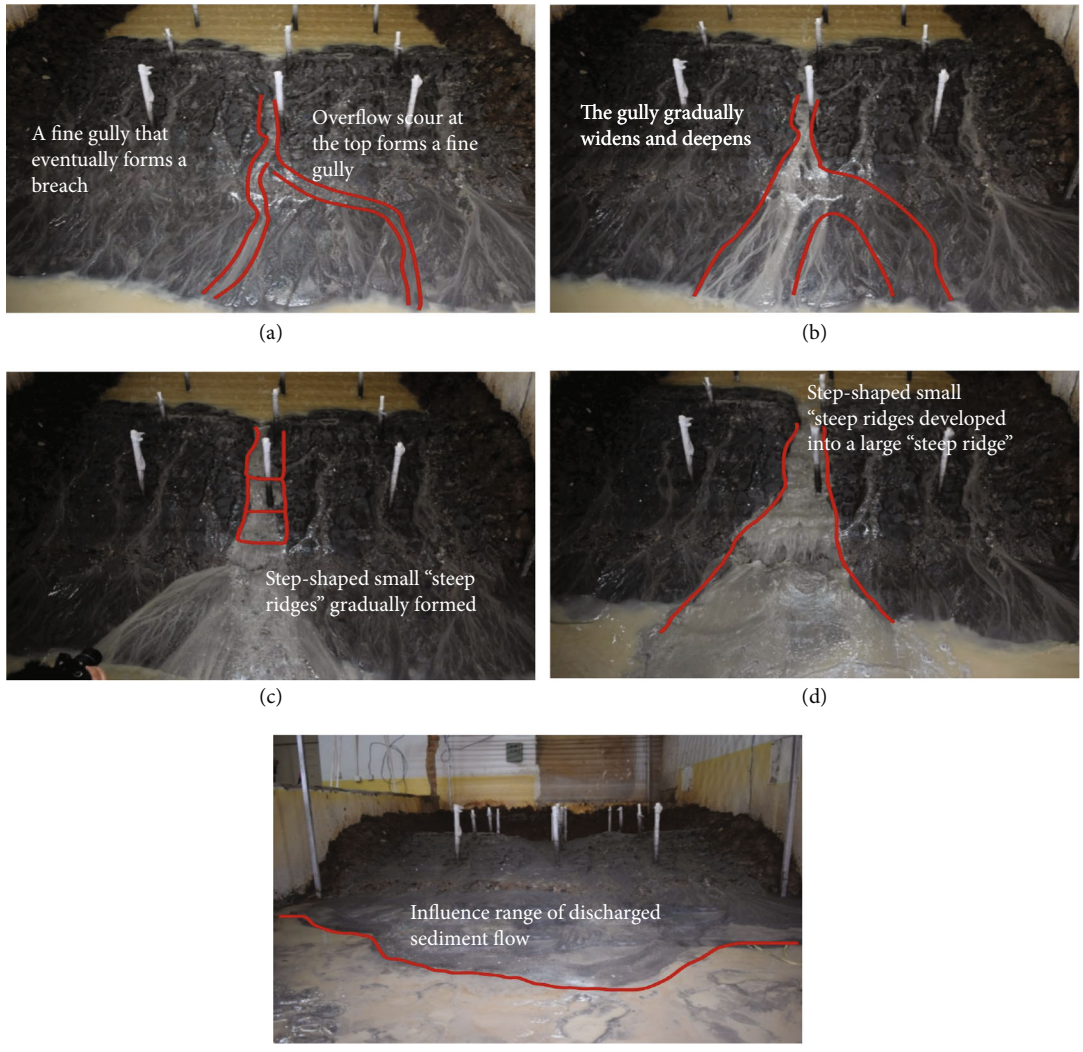

Figure 11: Tailing dam break breach evolution.

Table 2: The depth and width change of the breach.

Dam failure time (min)	Width (mm)	Depth (mm)
1	10.2	3.2
2	27.75	6.5
3	55.35	9.8
4	80.86	12.5
5	120.78	20.5
6	220.85	32.8
7	300.1	44.9
8	318.5	56.8
9	323.2	58.7
10	338.76	59.2
11	340.58	63.1

middle period of the dam failure, the increase rate of the width and depth increased rapidly (corresponding to Figures 11(c) and 11(d)), which was mainly related to the rapid increase of the breach flow. The erosion ability of the water flow reached the maximum, and the widening and deepening rates of the breach reached the maximum when the steep developed upstream of the dam body and approached the bottom of the breach. At this stage, the widening rate of the breach was much larger than the deepening rate, which was about 3-8 times the deepening rate. This was mainly because the widening of the breach was related to not only the tailing migrated by the water flow scouring but also the water flow erosion. The deepening of the breach depth resulted in intermittent instability and collapse of the breach on both sides, and the width of the breach developed rapidly. In the late period of dam failure, the widening and deepening rates of breach gradually decreased to zero (corresponding to Figure 11(e)). After the flood peak at the breach, the flow of the breach gradually decreased, and the water flow erosion to the breach was weakened. When the flow velocity of the flow at the breach was less than the starting velocity of the tailings, the widening and deepening development of the break stopped.

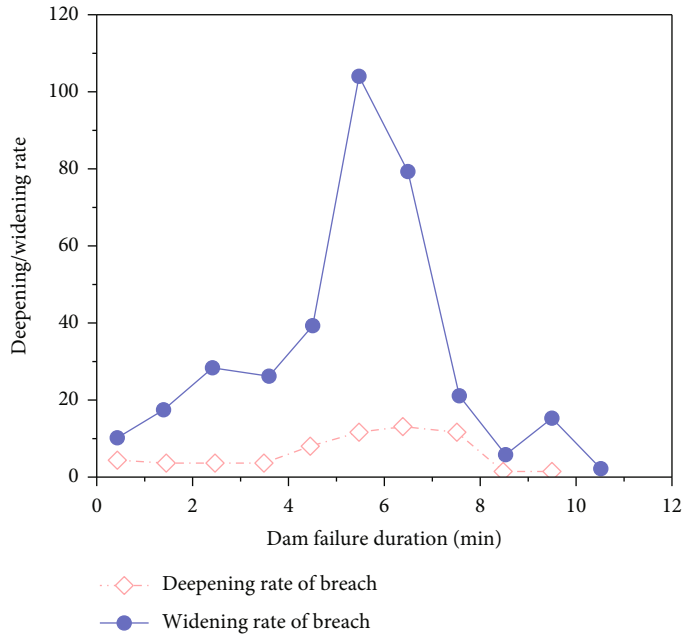

Figure 12: The variation of deepening and widening rate with a time of the breach.

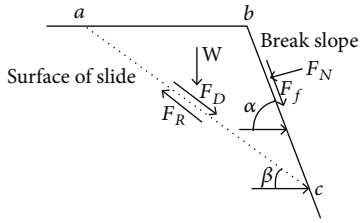

Figure 13: Analysis of side slope stability.

Figure 13 is the schematic diagram of slope stability analysis of breach, with *abc* as sliding soil and *ac* as a critical sliding surface.

According to the limit equilibrium theory, the stability safety factor of breach slope is assumed to be F_S.

$$F_S = \frac{F_R}{F_D}. \tag{2}$$

F_R is the soil antisliding force, and F_D is the soil sliding force, in which

$$F_R = W\cos\beta\tan\phi + F_N\cos(\alpha-\beta)\tan\phi + F_f\sin(\alpha-\beta), \tag{3}$$

$$\tan\phi = cl_{ac} + c\frac{1}{2}L_{ac}L_{bc}\sin(\alpha-\beta), \tag{4}$$

$$F_D = W\sin\beta - F_N\sin(\alpha-\beta) + F_f\cos(\alpha-\beta). \tag{5}$$

Equations (3) and (5) are brought into Eq. (2) for calculation. When the breach slope is in the critical state of collapse, the breach slope was in a stable state and would not collapse, where W is the gravity of the sliding soil, β is the angle between the sliding surface and the horizontal plane, φ is the internal friction angle of the soil, F_N is the hydrostatic pressure, α is the angle between the slope of the breach slope and the horizontal plane, F_f is the friction force of the water flow on the side wall, c is the cohesion of the soil, *ac* are the length of the sliding surface, and *bc* are the length of the sliding slope.

It is indicated that water flow erosion is the dominant factor in the development of the breach, and the development process of the breach can be calculated according to the erosion formula. The formula for the sediment transport rate is

$$Q_s = \frac{(1-n)V}{\Delta t}, \tag{6}$$

$$Q_s = q_s cs, \tag{7}$$

$$V = bcL, \tag{8}$$

where Q_s is the total transport sand rate, q_s is the unit transport sand, n is the porosity, V is the total volume of transport sand during Δt, c is the wetted perimeter of breach, L is the length of current scour, and b is the width of current scour.

Combining Equations (6) to (8), the erosion width of the breach during the erosion process of the dam body can be obtained.

$$b = \frac{\Delta t q_s}{(1-n)L}, \tag{9}$$

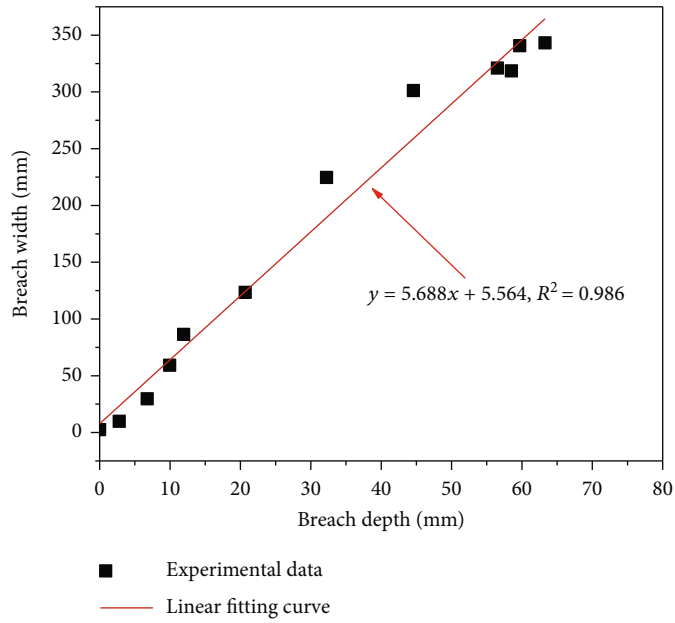

Figure 14: The relation curve of width and depth variation of breach in different stages.

where

$$q_s = 0.05v^2\left(\frac{d_{50}}{g(d_r-1)}\right)^{0.5}\left(\frac{\tau}{p_w g(d_r-1)d_{50}}\right)^{1.5}, \quad (10)$$

where g is the gravitational acceleration, τ is the shear stress, d_r is the relative density, d_{50} is the median size, β_w is the water density, and v is the velocity of water flow.

Substitute Equation (10) into Equation (9) to obtain

$$b = 0.05\frac{\Delta t v^2}{(1-n)L}\left(\frac{d_{50}}{g(d_r-1)}\right)^{0.5}\left(\frac{\tau}{p_w g(d_r-1)d_{50}}\right)^{1.5}. \quad (11)$$

The erosion width variation rate of the breach is

$$\frac{\mathrm{db}}{\mathrm{dh}} = 0.05v^2\left(\frac{d_{50}}{g(d_r-1)}\right)^{0.5}\left(\frac{\tau}{p_w g(d_r-1)d_{50}}\right)^{1.5}L^{-1}(1-n)^{-1}. \quad (12)$$

Plot the breach width and depth in different time periods as a curve, as shown in Figure 14.

It can be seen from Figure 14 that the width and depth of the breach show a certain linear relationship during the dam failure process, and the width and depth of the breach are positively correlated, as follows:

$$\frac{\mathrm{db}}{\mathrm{dh}} = k, \quad (13)$$

where h is the breach depth, and k is the ratio of widening rate to deepening rate of breach. According to the measured data of this test, it can be seen that the value of k ranges from 3 to 8.

It can be drawn from Equation (12) that the breach development mainly depended on the dam body scour induced by the water and sand flow, and the scour resistance of the dam body was mainly related to factors such as the flow velocity, the dam material, and the material density. From the development process of the breach shape at the dam crest, it was indicated that the breach widening took a dominant position in the development of the burst. In particular, in the middle stage of dam failure, the flow rate of the breach increased rapidly, and the water flow erosion was severe.

3.3.3. Variation of Dam Body Elevation before and after Dam Failure. After the dam failure, the variation of dam body elevation before and after dam failure was measured by the laser range finder, as shown in Figure 15. The dam failure variation body before and after the dam failure could be obtained from the difference.

(1) The elevation of the dam body expressed obvious changes before and after the dam collapse, and the dam body elevation change was the smallest at the location of "horizontal monitoring line 1" (the initial dam crest position). However, the dam body elevation changes were obvious at the positions of "horizontal monitoring line 2," "horizontal monitoring line 3," and "horizontal monitoring line 4" (between the subdams of the dam body)

(2) A breach occurred near the middle of the dam crest (that was where the monitoring points 4-1, 4-2, 4-3, and 4-4 were located), and the variation of dam body elevation at the breach reached the maximum. After

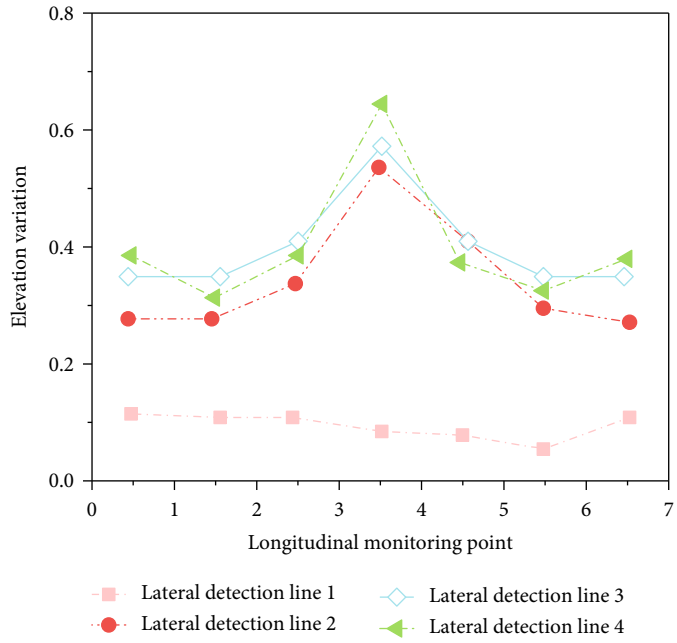

Figure 15: The height variation of dam break before and after dam failure.

the collapse, the shape of the breach was parabolic, and the maximum value of the parabola was the deepest part of the breach

Under the full-scale rainfall condition, the dam body was subjected to the combined erosion of rainfall flow and overflow, resulting in migration of partial tailings and forming gullies on the surface of the dam body. Due to the continuous infiltration and seepage of water level in the dam body, the elevation of the dam body at the four subdam positions changed obviously. At the downstream of the dam body, part of the tailings was carried to the downstream of the dam body for accumulation because of the sand-carrying effect of the water flow. The elevation of the dam crest at the initial stage after and before dam collapse had no obvious change.

With the rise of the water level in the tailing pond, the water level exceeded the lowest point of the dam crest, and a breach occurred near the middle of the dam crest. The water flow in the tailing pond constantly flew out of the pond through the breach, and the flow rate and sand-carrying capacity at the breach reached the maximum. At the same time, the scouring effect of the water flow at the breach reached the maximum. The tailings at the breach were carried downstream by the water flow under the continuous scouring action of the water flow, resulting in the largest change in the elevation of the dam body at the breach.

4. Conclusions

The indoor model test is an important scientific method for some complex engineering problems, because it can reproduce various phenomena and problems of the prototype. It is available for tests to control the test conditions and parameters, simplify the test, and shorten the research period. In this paper, the collapse mechanism of tailing dam overflow and the whole process of collapse expansion under the full-scale rainfall condition were analyzed through the indoor model test of the tailing dam. The research results show the following:

(1) During the scattered discharge tailings process in front of the dam, the tailing slurry flows in the state of "thin flow" and "laminar flow," forming a clear fan-shaped alluvial beach in front of the dam. During the deposition of the tailings on the dry beach, the tailings showed obvious particle size classification. The farther from the subdam, the finer the tailing particle size

(2) The variation of the water level in the tailing pond during the rainfall had a significant impact on the variation of the height of the infiltration line. At different times of rainfall, the height of the infiltration line at different positions of the dam body varies. Before 3600 s of rainfall, the height of the infiltration line obviously lagged behind the water level height. In addition, the hysteresis effect from the tail of the tailing pond to the dam body became more obvious. After 3600 s of rainfall, the response of the height of the infiltration line to the water level change was obvious, and the phenomenon that the height of the infiltration line lagged behind the height of the water level basically disappeared

(3) Under the rainfall condition, the indoor dam overtopping failure process of tailing dam mainly experienced the following five periods: dam body flooding (gully erosion), formation of multistep small "steep

ridges," formation of large "steep ridges," the rapid expansion of the breach, and complete collapse of the dam body (in the shape of a fan)

(4) In the process of dam failure, there is a certain positive linear relationship between the width and depth of the dam crest breach in different periods. Water flow erosion was the dominant factor in the development and change of the breach. During the dam breach, the variation in the width of the breach was greater than the variation in the depth of the breach, and the breach widening rate was about 3 to 8 times the deepening rate. In the middle period of the dam collapse, the lateral widening of the failure dominated the development of the breach failure

(5) The dam body had obvious elevation change after the dam failure, and the elevation change was the smallest at the initial dam crest. The elevation change between the dam body and the subdams was more obvious. After the dam collapses, the reach shape was parabolic, and the dam elevation change at the breach reached the maximum

Data Availability

The data that support the findings of this study are available from the submitting author upon reasonable request.

Conflicts of Interest

The authors declare that they have no conflicts of interest.

Acknowledgments

This study was partially funded by the National Natural Science Foundation of China (No. 52174114), Open Fund Project of the National Engineering and Technology Research Center for Development &Utilization of Phosphate Resources (No. NECP2022-07), State Key Laboratory of Hydroscience and Engineering of Tsinghua University (No. 61010101218), and Yunnan International Technology Transfer Center for Mineral Resources Development and Solid Waste Resource Utilization (202203AE140012).

References

[1] T. Wang, Y. Zhou, Q. Lv, Y. Zhu, and C. Jiang, "A safety assessment of the new Xiangyun phosphogypsum tailings pond," *Minerals Engineering*, vol. 24, no. 10, pp. 1084–1090, 2011.

[2] G. Yin, X. Jing, W. Zhang, and X. Li, "Experiments of debris flow disaster of tailings dam-break," *Disaster Advances*, vol. 4, pp. 4–9, 2011.

[3] A. T. Lima, F. A. Bastos, F. J. Teubner, R. R. Neto, A. Cooper, and G. F. Barroso, "Strengths and weaknesses of a hybrid post-disaster management approach: the Doce River (Brazil) mine-tailing dam burst," *Environmental Management*, vol. 65, no. 6, pp. 711–724, 2020.

[4] D. Ma, J. Zhang, H. Duan et al., "Reutilization of gangue wastes in underground backfilling mining: overburden aquifer protection," *Chemosphere*, vol. 264, Part 1, article 128400, 2021.

[5] X.-T. Ai, G.-J. Wang, X.-Y. Kong, B. Cui, B. Hu, and H. Ma, "The Scale Effect of Coarse-Grained Materials by Triaxial Test Simulation," *Advances in Civil Engineering*, vol. 2021, Article ID 6665531, 13 pages, 2021.

[6] Z. Dou, Y. Liu, X. Zhang et al., "Influence of layer transition zone on rainfall-induced instability of multilayered slope," *Lithosphere*, vol. 2021, no. Special 4, article 2277284, 2021.

[7] X. Li, Q. Li, Y. Hu et al., "Study on three-dimensional dynamic stability of open-pit high slope under blasting vibration," *Lithosphere*, vol. 2022, no. Special 4, article 6426550, 2021.

[8] X. T. Ai, G. J. Wang, and C. Zhang, "Stability analysis of high dump with wide graded waste rock," *Rock and Soil Mechanics*, vol. 30, no. 11, pp. 3777–3788, 2020.

[9] J. Wang, D. Ma, Z. Li, Y. Huang, and F. Du, "Experimental investigation of damage evolution and failure criterion on hollow cylindrical rock samples with different bore diameters," *Engineering Fracture Mechanics*, vol. 260, article 108182, 2022.

[10] D. Ma, S. Kong, Z. Li, Q. Zhang, Z. Wang, and Z. Zhou, "Effect of wetting-drying cycle on hydraulic and mechanical properties of cemented paste backfill of the recycled solid wastes," *Chemosphere*, vol. 282, article 131163, 2021.

[11] G. Wang, B. Hu, S. Tian, M. Ai, W. Liu, and X. Kong, "Seepage feld characteristic and stability analysis of tailings dam under action of chemical solution," *Scientific Reports*, vol. 11, no. 1, article 4073, 2021.

[12] G. Wang, S. Tian, B. Hu, X. Kong, and J. Chen, "An experimental study on tailings deposition characteristics and variation of tailings dam saturation line," *Geomechanics and Engineering*, vol. 23, no. 1, pp. 85–92, 2020.

[13] B. Cui, G. Wang, W. Liu et al., "Seepage and stability analysis of pore air pressure on a high-bench dump under heavy rainfall," *Chinese Journal of Engineering*, vol. 43, no. 3, pp. 365–375, 2021.

[14] G. Wang, S. Tian, B. Hu, Z. Xu, J. Chen, and X. Kong, "Evolution pattern of tailings flow from dam failure and the buffering effect of debris blocking dams," *Water*, vol. 11, no. 11, pp. 2388–2401, 2019.

[15] L. Clarkson and D. Williams, "An overview of conventional tailings dam geotechnical failure mechanisms," *Mining, Metal-lurgy & Exploration*, vol. 38, no. 3, pp. 1305–1328, 2021.

[16] W. Hu, C. L. Xin, Y. Li, Y. S. Zheng, T. W. J. van Asch, and M. McSaveney, "Instrumented flume tests on the failure and fluidization of tailings dams induced by rainfall infiltration," *Engineering Geology*, vol. 294, no. 5, article 106401, 2021.

[17] S.-Q. Lin, G.-J. Wang, W.-L. Liu et al., "Regional distribution and causes of global mine tailings dam failures," *Metals*, vol. 12, no. 6, p. 905, 2022.

[18] M. Rico, G. Benito, A. R. Salgueiro, A. Díez-Herrero, and H. G. Pereira, "Reported tailings dam failures: a review of the European incidents in the worldwide context," *Journal of Hazardous Materials*, vol. 152, no. 2, pp. 846–852, 2008.

[19] M. T. Zandarín, L. A. Oldecop, R. Rodríguez, and F. Zabala, "The role of capillary water in the stability of tailing dams," *Engineering Geology*, vol. 105, no. 1-2, pp. 108–118, 2009.

[20] P. Lade and J. Yamamuro, "Evaluation of static liquefaction potential of silty sand slopes," *Canadian Geotechnical Journal*, vol. 48, no. 2, pp. 247–264, 2012.

[21] C. D. Anderson and T. L. Eldridge, "Critical state liquefaction assessment of an upstream constructed tailings sand dam," , CRC Press, 1st edition, 2011.

[22] G. J. Hanson, K. R. Cook, and S. L. Hunt, "Physical modeling of overtopping erosion and breach formation of cohesive embankments," *Transactions of the ASABE*, vol. 48, no. 5, pp. 1783–1794, 2005.

[23] C. Debarghya and C. Deepamkar, "Investigation of the behavior of tailings earthen dam under Seismic conditions," *American Journal of Engineering & Applied Sciences*, vol. 2, no. 3, pp. 559–564, 2009.

[24] A. Gens and E. E. Alonso, "Aznalcóllar dam failure. Part 2: stability conditions and failure mechanism," *Geotechnique*, vol. 56, no. 3, pp. 185–201, 2006.

[25] A. R. Salgueiro, H. G. Pereira, M. T. Rico, G. Benito, and A. Díez-Herreo, "Application of correspondence analysis in the assessment of mine tailings dam breakage risk in the Mediterranean region," *Risk Analysis*, vol. 28, no. 1, pp. 13–23, 2008.

[26] K. Wang, P. Yang, K. A. Hudson-Edwards, W. Lyu, C. Yang, and X. Jing, "Integration of DSM and SPH to model tailings dam failure run-out slurry routing across 3D real terrain," *Water*, vol. 10, no. 8, article 1087, 2018.

[27] Y. Zhuang, K. Jin, Q. Cheng, A. Xing, and H. Luo, "Experimental and numerical investigations of a catastrophic tailings dam break in Daye, Hubei, China," *Bulletin of Engineering Geology and the Environment*, vol. 81, no. 9, 2022.

[28] M. Rico, G. Benito, and A. Díez-Herrero, "Floods from tailings dam failures," *Journal of Hazardous Materials*, vol. 154, no. 1-3, pp. 79–87, 2008.

[29] C. Zhu, M. C. He, M. Karakus, X. B. Cui, and Z. G. Tao, "Investigating toppling failure mechanism of anti-dip layered slope due to excavation by physical modelling," *Rock Mechanics and Rock Engineering*, vol. 53, no. 11, pp. 5029–5050, 2020.

[30] T. Wu and J. Qin, "Experimental study of a tailings impoundment dam failure due to overtopping," *Mine Water and the Envi-ronment*, vol. 37, no. 2, pp. 272–280, 2018.

[31] M. L. Dong, P. H. S. W. Kulatilake, and F. Zhang, "Deformation and stability investigations in 3-D of an excavated rock slope in a hydroelectric power station in China," *Computers and Geotechnics*, vol. 96, pp. 132–149, 2018.

[32] J. Jin, C. Song, B. Liang, Y. Chen, and M. Su, "Dynamic characteristics of tailings reservoir under seismic load," *Environmental Earth Sciences*, vol. 77, no. 18, p. 654, 2018.

[33] P. Zhang, D. Zhang, Y. Yang et al., "A case study on integrated modeling of spatial information of a complex geological body," *Lithosphere*, vol. 2022, article 2918401, no. Special 10, 2022.

[34] W. Shuaifeng, C. Hong, X. Jianzhang, Y. J. Du Jifang, L. Chuanpeng, and Z. BinBin, "Experimental study on discharge impact characteristics induced by piping failure of tailings dam," *Arabian Journal of Geosciences*, vol. 14, no. 2054, article 2054, 2021.

[35] A. L. Li, "Tailings subaerial and subaqueous deposition and beach slope modeling," *Journal of Geotechnical and Geoenvironmental Engineering*, vol. 141, no. 1, article 04014089, 2015.

[36] N. T. Ozcan, R. Ulusay, and N. S. Isik, "A study on geotechnical characterization and stability of downstream slope of a tailings dam to improve its storage capacity (Turkey)," *Environmental Earth Sciences*, vol. 69, no. 6, pp. 1871–1890, 2013.

[37] C. Liu, Z. Shen, L. Gan, L. Xu, K. Zhang, and T. Jin, "The seepage and stability performance assessment of a new drainage system to increase the height of a tailings dam," *Applied Sciences*, vol. 8, no. 10, p. 1840, 2018.

[38] S. Wang, G. Mei, X. Xie, and L. Guo, "The influence of the instantaneous collapse of tailings pond on downstream facilities," *Advances in Civil Engineering*, vol. 2021, Article ID 4253315, 15 pages, 2021.

[39] Z. Tian, H. Yang, W. Wang, and D. Cao, "Numerical analysis of sand bed degrading and sediment transport rate under tailings dam break," *Frontiers in Earth Science*, vol. 9, article 686277, 2021.

[40] Z. A. Wei, *Research on the Characteristics and Dam Stability of Fine Grained Tailings*, Chongqing University, 2004.